Materials & Design 226 (2023) 111596

Contents lists available at ScienceDirect

Materials & Design

journal homepage: www.elsevier.com/locate/matdes

A novel design method to produce 3D auxetic metamaterials with continuous pores exemplified through 3D rotating auxetic systems

Russell Galea [a], Pierre-Sandre Farrugia [a,b], Krzysztof K. Dudek [c], Daphne Attard [a], Joseph N. Grima [d], Ruben Gatt [a,e,*]

[a] Metamaterials Unit, Faculty of Science, University of Malta, Msida MSD 2080, Malta
[b] Department of Geosciences, Faculty of Science, University of Malta, Msida MSD 2080, Malta
[c] Institute of Physics, University of Zielona Gora, ul. Szafrana 4a, Zielona Gora 65-069, Poland
[d] Department of Chemistry, Faculty of Science, University of Malta, Msida MSD 2080, Malta
[e] Centre for Molecular Medicine and Biobanking, University of Malta, Msida MSD 2080, Malta

HIGHLIGHTS

- A novel method to produce 3D auxetic metamaterials has been proposed.
- The proposed method involved the application of continuous voids with constant cross-sectional area in multiple perpendicular planes.
- The potential of using subtractive manufacturing, additive manufacturing, or casing to fabricate these 3D auxetic structures was shown.
- Using continuous voids with a diamond shaped cross-sectional area were shown to produce novel 3D auxetic structures.
- Nonlinear simulations and experimental testing showed that the Poisson's ratio of these structures is strain independent up to 7% deformation.

GRAPHICAL ABSTRACT

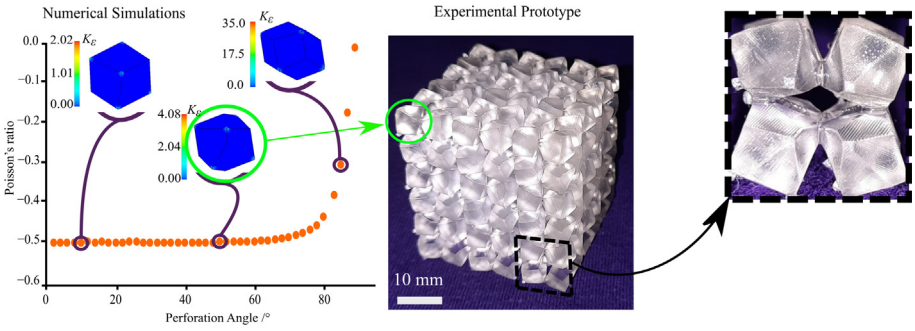

ARTICLE INFO

Article history:
Received 20 June 2022
Revised 17 December 2022
Accepted 3 January 2023
Available online 4 January 2023

Keywords:
Perforations
Subtractive manufacturing
Negative Poisson's ratio
3D auxetic structures

ABSTRACT

Prototyping of three-dimensional mechanical metamaterials that exhibit negative Poisson's ratio is usually performed through additive manufacturing. Although this technique has a huge potential, its use to engineer mechanical metamaterials for consumer products is still challenging. In this work, a novel design method is being proposed where 3D auxetic metamaterials can be produced by introducing continuous voids of constant cross-sectional area. Such voids would be inserted at strategic positions in different perpendicular planes of a solid block to obtain a continuous three-dimensional mechanical metamaterial that can exhibit the desired mechanical characteristics. The use of continuous voids to design the 3D meatamaterial makes it possible to use additive manufacturing, subtractive manufacturing as well as casting to produce these systems. The proposed design method is explained by using continuous voids having a diamond shaped cross-sectional area. The resulting group of structures can be described as connected polygons and were found to exhibit a negative or zero Poisson's ratio. The

* Corresponding author.
E-mail addresses: russell.galea.15@um.edu.mt (R. Galea), pierre-sandre.farrugia@um.edu.mt (P.-S. Farrugia), k.dudek@if.uz.zgora.pl (K.K. Dudek), daphne.attard@um.edu.mt (D. Attard), joseph.grima@um.edu.mt (J.N. Grima), ruben.gatt@um.edu.mt (R. Gatt).

https://doi.org/10.1016/j.matdes.2023.111596

analysed systems were also found to have a strain independent Poisson's ratio up to at least 7% strain. The proposed design method can thus facilitate the availability of three dimensional auxetic metamaterials in the consumer market which to date is conspicuous by their absence.

1. Introduction

Technological advancement is at least partly dependent on the development of new materials with novel functionalities that lead to innovative products. At present, one of the most promising ways of designing systems with improved functionalities is based on the use mechanical metamaterials. These are engineered materials that exhibit behaviours not commonly found in nature such as negative Poisson's ratios [1], negative compressibility [2], and negative stiffness [3]. Their abilities are mainly dependent on their geometry and deformation mechanism [4]. An important subset of mechanical metamaterials which has attracted significant attention in the past few decades is represented by auxetic systems [5], i.e. materials characterised by a negative Poisson's ratio (NPR). This type of mechanical metamaterials will contract (expand) transversely when subjected to a uniaxial compressive (tensile) force. This behaviour is unlike that of conventional materials which expand transversely in response to a compressive force [6].

The presence of an NPR is associated with several desirable material properties including superior shear [7], indentation [8,9], impact [10], and fracture [11] resistance, as well as better energy absorption performance [12–14] as compared to materials with positive Poisson's ratio. Furthermore, NPR systems can have a variable permeability [15] and exhibit synclastic curvature [16–18]. For this reason, it is expected that auxetic materials and structures can be used to design innovative products having an improved performance across a number of industries including, but not limited to, the biomedical [19], textiles [20,21] (particularly for sport applications [16,18]), automotive [22–24], and aerospace[17] ones. Examples of such products comprise vibration dampers [22–24], smart sensors [25,26], adaptable body armour [10], seat cushions [27], smart filters [15,28], acoustic isolators [29], and magnetic auxetic system s[30,31] such as thin memory films [32]. They can also be used for applications where impact [10], indentation, and fatigue resistance [33,34] are required.

A significant advancement in auxetic research was attained with the development of 3D systems that are capable of exhibiting an NPR behaviour in at least two planes that are orthogonal to each other (henceforth referred to as 3D auxetic systems). One such system is the three-dimensional rotating rigid cuboids structure proposed by Attard and Grima [35]. This structure is capable of exhibiting an NPR along some planes depending on the angle between the cuboids. The design concept was subsequently extended by Kim et al. [36] who studied the Poisson's ratio of 3D structures made of interconnected triangular, hexagonal, or square prisms [36]. Other 3D auxetic designs that have been proposed include the 3D arrowhead system [23,37], 3D re-entrant systems [38,39], 3D chiral systems [40,41], interacting particles [42–44], random networks [45], and 3D buckling soft metamaterials [46,47]. Research on 3D auxetic systems has only flourished recently possibly because the complex geometries involved are difficult to manufacture, limiting their industrial applicability. The situation has changed with the evolution of additive manufacturing which allows the fabrication of 3D auxetic metamaterials with relative ease. In fact, additive manufacturing is possibly-one of the best fabrication methods for such structures, notwithstanding the number of challenges this technique presents, which include production time, void formation, anisotropic microstructure, and mechanical properties [48].

However, additive manufacturing is not the only method that has been useful to produce auxetic structures. In fact, subtractive manufacturing has been successfully employed for the fabrication of 2D auxetic metamaterials (i.e. materials which show a negative Poisson's ratio in just one plane). The method involves the perforation of a sheet of conventional material (that has positive Poisson's ratio) at strategic loci [29,49]. In consequence, it has been the focus of extensive research in recent times [50–59] due to the ease and simplicity with which 2D auxetic structures can be produced. Various perforation shapes have been adopted to re-create known 2D auxetic structures [1,60–69], including star, diamond (rhombus), elliptical, rectangular, and hexagonal ones, leading to systems mimicking the rotating rigid triangles [50,70], rotating rigid quadrilaterals [29,49,51,53,54,71,72], and chiral systems [52,53,64–66,73–77]. It has also been shown that slit and / or I-shaped perforations may be used to obtain systems resembling the 2D re-entrant, chiral, and rotating rigid units mechanisms [54,74,78]. Furthermore, subtractive manufacturing has also been used to produce 2D hierarchical auxetic metamaterials [79,80].

Notwithstanding the amount of research in 3D auxetics and 2D perforated auxetic systems, to date, no attempt has been made to propose a design method that can be used to produce 3D auxetic metamaterials having continuous voids of constant cross-sectional area. The structures obtained from such a design method would be able to be produced through various methods, including subtractive manufacturing, additive manufacturing and casting. Such systems would combine the advantages specific to 3D auxetic structures [81] with multiple streamlined production processes, depending on the case. In view of these considerations, a novel design method will be proposed in this study which utilises the application of continuous voids of constant cross-sectional area on different planes of a solid block of material. This process will be exemplified by using continuous voids having a diamond shaped cross-sectional area. It will be shown for the first time that several 3D auxetic metamaterials, having negative or zero Poisson's ratios can be obtained using such diamond shaped voids.

2. Methodology

2.1. Description of the proposed design method used to produce 3D auxetic metamaterials with continuous voids

In this section a description of how auxetic metamaterials may be produced through the proposed novel design method will be given. To achieve this, continuous voids having a diamond shape perforation will be used as an example (*see* Fig. 1). For ease of reference, the continuous voids having a constant cross-sectional area will henceforth be referred to as 'perforations'. Referring to Fig. 1 (a), without loss of generality, starting from a cube made of conventional material, a first set of perforations can be carried out on the *xy*-plane using equally sized diamond shaped perforations (i.e. all diamond shaped perforations have equal side lengths). The perforations traverse the whole length of the material which is orthogonal to the *xy*-plane, i.e. that is aligned along the *z*-axis. Once applied, the pattern of perforations is such that the nearest neighbouring rhombi are rotated by 90° with respect to each other, meaning that their longest diagonals are aligned along perpendicular directions. At the same time, the nearest corners of the dia-

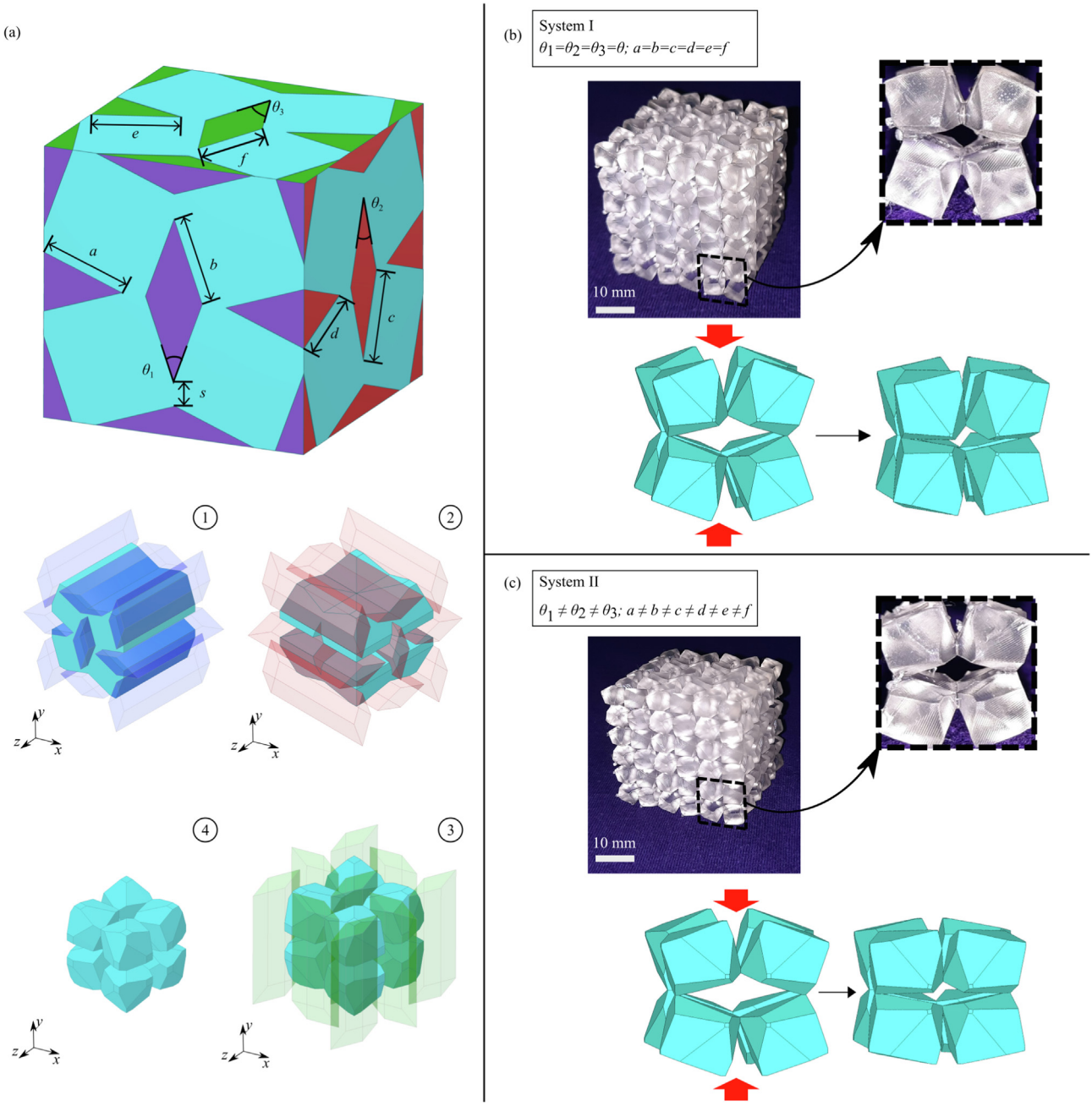

Fig. 1. (a) Production of 3D perforated systems using continuous voids having a diamond shaped cross-sectional area (b) An example of a regular 3D perforated system and (c) an example of a perforated system using different size continuous diamond shaped voids.

mond shaped perforations are separated by an equal distance *s*. This is required to provide spacing material so as to connect the different rigid units. The resultant structure mimics the 2D rotating squares system [49]. Thus, provided that *s* is small enough, the system is expected to show a negative Poisson's ratio in the *xy*-plane.

A second set of analogous perforations can then be performed in the *yz*-plane. This will result in a system which has a projected 'rotating squares' geometry in both the *xy*- and *yz*-planes. It would thus be expected that such a system will exhibit a negative Poisson's ratio in both planes. To complete the structure, a third set of analogous perforations is performed in the *xz*-plane, yielding the 3D polygons system shown in Fig. 1(b). Based on the previous considerations, the resulting system is expected to exhibit a negative Poisson's ratio when loaded in all three planes.

The concept outlined above can easily be extended to one where the diamond shaped perforations are not the same. To do this, diamond perforations having different side length and internal angles need to be used as illustrated in Fig. 1(c). In this case, it is expected that the Poisson's ratio will depend on the dimensions of the diamond perforations used in each orthogonal plane, meaning that it can vary between planes.

2.2. Geometric considerations of the proposed design method used to produce 3D auxetic metamaterials with continuous voids

In the case of the proposed design method, one must ensure that the perforations performed on one plane do not cut through the material between the different units of another plane as this would result in disjointed parts. The geometric requirements for

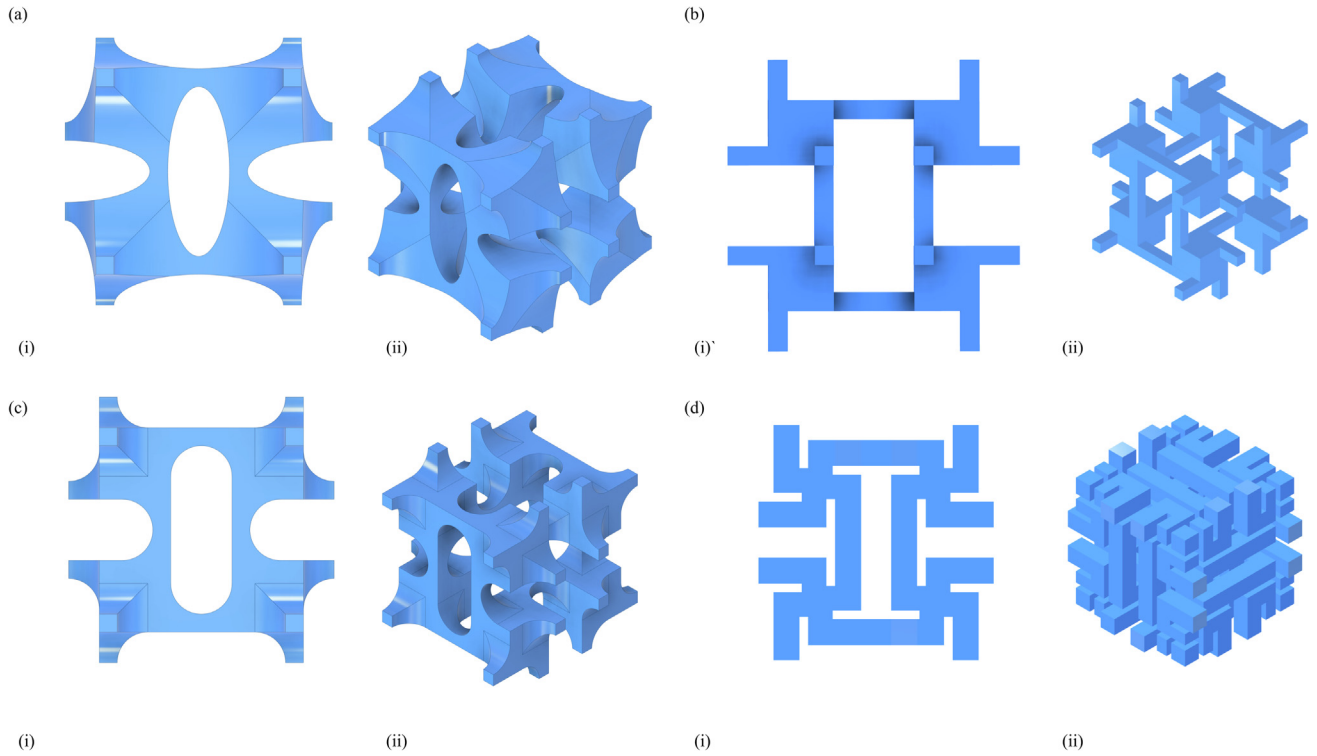

Fig. 2. An illustration possible 3D auxetic structure that may be obtained when using different perforation shapes. Panel (i) represents the projections of the 3D structures in the major planes while panel (ii) shows the 3D structure.

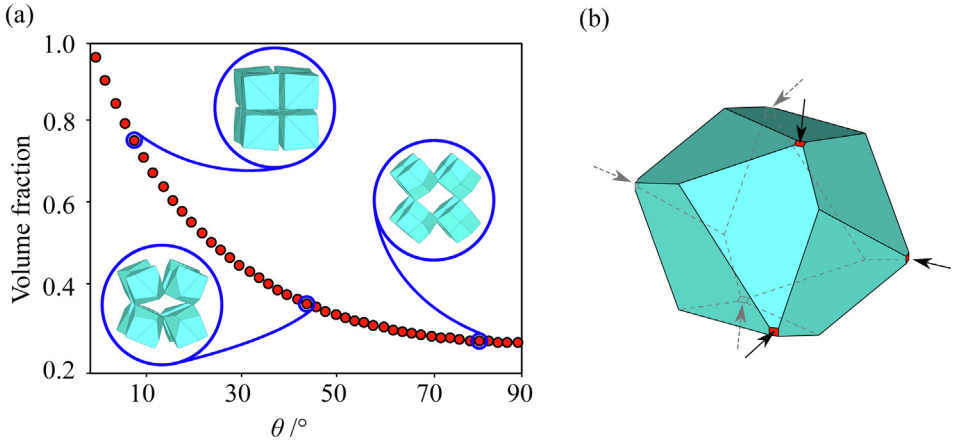

Fig. 3. (a) Volume fraction against perforation angle with the insets showing structures having a perforation angle, θ, of 10°, 45°, and 80°. (b) An irregular dodecahedron obtained by taking one eighth of a unit cell (θ = 50°).

the diamond shaped perforations used in this study as an example of the proposed design method are given in this section. The diamond shaped perforations which can be applied to each major plane of a block of material is characterised by the side lengths and internal angles of the diamond/rhombi shaped perforation as well as the separation between the nearest corners of the perforations s. Given the existent relations between the internal angles of a rhombi, only one angle needs to be specified for each plane. This will be referred to as the aperture angle. Considering the simplest case proposed here, whereby all the side length of the rhombi are equal to a, and the aperture angle in each plane is also equal, and referenced by θ, the side lengths of the unit cell along the x, y, and z directions are given respectively by:

$$X = Y = Z = 2\left\{a\left[\cos\left(\frac{\theta}{2}\right) + \sin\left(\frac{\theta}{2}\right)\right] + s\right\} \tag{1}$$

The resultant perforated system will henceforth be referred to as the regular 3D perforated system.

In the case that rhombi of different dimensions and internal angles are used, as indicated in Fig. 1(c), the side lengths of the unit cell along the x, y, and z directions are given respectively by:

$$X = 2\left[a\cos\left(\frac{\theta_1}{2}\right) + b\sin\left(\frac{\theta_1}{2}\right) + s\right] \tag{2}$$

$$Y = 2\left[a\sin\left(\frac{\theta_1}{2}\right) + b\cos\left(\frac{\theta_1}{2}\right) + s\right] \tag{3}$$

$$Z = 2\left[d\cos\left(\frac{\theta_2}{2}\right) + c\sin\left(\frac{\theta_2}{2}\right) + s\right] \tag{4}$$

Here a and b are the side lengths of the rhombi in the xy-plane while c and d are those in the yz-plane (Fig. 1. (a)(i)). In addition θ_1 and θ_2 are receptively the aperture angles in the xy and yz planes. Geometric analysis shows that the c, d, and θ_2 are related to each other as well as to the corresponding parameters in the xy-plane through the equations,

$$\theta_2 = 2\cos^{-1}\left[\frac{b\cos\left(\frac{\theta_1}{2}\right)}{c}\right] \tag{5}$$

$$d = \frac{a\sin\left(\frac{\theta_1}{2}\right)}{\sin\left(\frac{\theta_2}{2}\right)} \tag{6}$$

It can be noted from Equation (5) that when $c = b\cos\left(\frac{\theta_1}{2}\right)$, the angle θ_2 is equal to zero, implying that no perforations can be made. In practice this sets a minimum value for c, as this side length must be larger than $b\cos\left(\frac{\theta_1}{2}\right)$.

In a similar way, the side lengths of the rhombi in the xz-plane, namely e and f, and the aperture angle θ_3 are related to the previously defined parameters through the equations,

$$e = \frac{b\sin\left(\frac{\theta_1}{2}\right)}{\sin\left(\frac{\theta_3}{2}\right)} \tag{7}$$

$$f = \frac{a\cos\left(\frac{\theta_1}{2}\right)}{\cos\left(\frac{\theta_3}{2}\right)} \tag{8}$$

$$\theta_3 = 2\tan^{-1}\left\{\frac{\min\left[c\sin\left(\frac{\theta_2}{2}\right), d\cos\left(\frac{\theta_2}{2}\right)\right]}{a\cos\left(\frac{\theta_1}{2}\right)}\right\} \tag{9}$$

where the function "min" returns the minimum of the input values. It should be mentioned that the definition of θ_3 has been chosen so as to prevent the perforations from cutting through the spacing material as this would remove the connection between the different units. This is not the only constraint that is needed to ensure that the geometry is not split up in disjointed parts. Testing has shown that the following relation also needs to hold:

$$f\cos\left(\frac{\theta_3}{2}\right) \le b\sin\left(\frac{\theta_1}{2}\right) + \frac{b\cos\left(\frac{\theta_1}{2}\right)}{\tan\left(\frac{\theta_1}{2}\right)} \tag{10}$$

The constraints mentioned need not be exhaustive of all possible ones. Identifying them would require a thorough investigation of all possible parameter space, something that was considered beyond the scope of the analysis.

The more general system being described here is thus characterised by six lengths (a, b, c, d, e, and f) and three angles (θ_1, θ_2, and θ_3) leading to a total of nine geometric parameters. In turn, these are related by five equations based on the geometric relations presented above. Hence, only four of the parameters are independent. Without loss of generality, these can be taken to be a, b, c and θ_1. The projections of each plane of the resulting 3D system may be described by Type I rotating rectangles system [72].

2.3. Finite element simulations

To study the mechanical properties of 3D structures produced through the design method proposed in this study, finite element simulations were performed on the 3D structures resulting when using diamond shaped perforations. As explained above, diamond shaped perforations were used as an example of the properties that can be obtained when using this design method. The mechanical properties of the novel 3D perforated systems were investigated using the Finite Element method, using the commercially available software ANSYS® Mechanical APDL Release 13. For the simulations, the symmetry that exists along lines parallel to the principal axes, passing through the middle of the connecting material between the polygons, were availed of. These lines of symmetry exist not only at the edges of the unit cell, but also midway through each side length of the original cuboid. Thus, only one eighth of the unit cell needed to be simulated. A benefit to using a reduced representative volume was a decreased simulation time.

The symmetry boundary conditions were imposed in a similar fashion to previous work [40]. To load the structure in the x direction, the nodes located on each face oriented along the zy plane were coupled to move together in the x-direction and equal compressive strains in the x direction were applied on the coupled nodes. Then the displacement of the nodes in the y direction on one of the faces oriented along the xz plane was set to zero, while the nodes on the opposite face were coupled to move together in the y direction. Similar boundary conditions were imposed on the nodes on the faces along the xy plane. This allowed the structure to be modelled as an infinite system, with the results providing the bulk properties of the material when loaded in the x direction. Inferentially, loading of the y, or z directions, were thus obtained by interchanging the boundary conditions (see supplementary information for a pictorial representation of the boundary conditions).

The element type for the simulation was set to SOLID187, this being a higher order 3D element with quadratic displacement behaviour that is able to model both elastic and plastic behaviour, as well as allowing for irregular meshes [82]. For the initial investigation, the Young's modulus was set to 1.1 GPa, while the Poisson's ratio was set to 0.45. Mesh independence tests were then carried out. The results indicated that using automatic (smart) element sizing with the finest mesh configuration, followed by a level 4 refinement around boundary nodes up to a depth of 3 elements inward from these nodes, produced results that were within 1 % of those obtained with a finer mesh (see supplementary information for more detailed results on the mesh independence tests). Hence, this configuration was chosen for the bulk of the simulations. It should be noted here that the adopted mesh density required extensive computational resources. In fact, simulating the whole of the unit cell with such a mesh density would not have been viable. Thus, the use of symmetry considerations to reduce the volume simulated to one eight of the unit cell was, in this case, necessary to obtain the needed results.

Initially a parametric analysis was carried out using linear simulations. The first set of these simulations sought to investigate the relation between the 'degree of openness' of the diamond shaped perforations and the mechanical properties (namely the Poisson's ratios and Young's moduli) of the regular 3D perforated system (System I). For the purpose, the following parameters were used (see Fig. 1(a)): $a = b = c = 10.0$ mm, $s = 0.5$ mm, while θ was varied between 1° and 90° in increments of 1°.

In the second set of simulations, the effect of s on the mechanical properties of System I was investigated. To do so, the following set of parameters was chosen: $a = b = c = 10.0$ mm, s was varied from 0.1 mm to 2.0 mm in increments of 0.1 mm, and angle θ was varied between the values of 10° to 80° in increments of 10°.

The third set of simulations considered the more general system. For this case, parameter a was set to 10.0 mm, parameters b and c were varied between 2.0 mm and 20.0 mm in increments of 2.0 mm, s was set at 0.5 mm while angle θ was assigned values from 10° to 80° in increments of 10°. The chosen parameter space allowed the investigation to have the aspect ratios of b/a and c/a span from relatively small to the relatively large values thus encompassing a wide variety of structures. Not all parameter combinations resulted in a tesselatable system due to the constraints mentioned.

From the numerical results obtained the engineering Poisson's ratio and Young's moduli in all loading directions were derived. Furthermore, the distribution of forces within the material was studied using the strain concentration factor (K_ε) which was defined as:

$$K_\varepsilon = \frac{\varepsilon_{max}}{\varepsilon_{ave}} \tag{11}$$

where ε_{max} is the von Mises strain at a specific region and ε_{ave} is the strain applied to the structure.

Based on the analysis of the initial parametric investigation, two structures were identified for further investigation. The first one represented the regular 3D perforated system having dimensions $a = b = c = 4.0$ mm and $\theta = 40°$, while the second one the more general cuboid system having dimensions $a = 4.0$ mm, $b = 4.8$ mm, $c = 4.8$ mm, and $\theta_1 = 40°$. These will be referred to as System I and System II respectively. Nonlinear simulations were carried out for these structures with the intention of comparing the results with those of the mechanical testing of physical prototypes. For the purpose, the mechanical properties of the material that was meant to be used for the manufacturing of the prototypes were determined from the mechanical testing of a number of dog bones (see supplementary information). The Poisson's ratio of the constituting material in the linear region was found to be 0.42 while the Young's modulus was estimated to be 1.52 MPa. Static simulations that take into consideration large deflections were then carried out. To do so, the stress–strain results obtained from the dog bones were used as inputs to the hyperelasticity model with the selection of the experimental response function model available in ANSYS APDL. The results could then be compared with those obtained through the mechanical testing of the prototypes. Details of the manufacturing and testing of the prototypes are given in the next section.

2.4. Experimental method

Experimental prototypes of 3D structures obtained by the design method proposed in this study when using diamond shaped perforations were also produced. This was achieved by applying the diamond shaped perforations in-silico and 3D printing the resultant 3D structure. 3D printing was done by using a Formlabs Form 3 SLA 3D printer using the Elastic 50A resin. The *xy* resolution was set to 100 μm and a layer thickness of 100 μm was adopted. Once printed the prototypes were washed with isopropyl alcohol (IPA) in the Formlabs Form Wash tank for 10 min. The parts were then removed from the build plate and washed once more for 10 min. Formlabs Form Cure was then used to cure the prototypes for 20 min at 60 °C. Once the process was completed, the structure dimensions (parameters a and b) and the separation between different perforations (parameter s) were measured. This was done using a Trinocular Stereo Microscope (HK 1Kins Technology Co ltd) mounted with a duly calibrated Industrial UHD 4 K SONY IMX334 HDMI Measuring Video Camera. One hundred measurements were taken for each parameter considered, from which the average, standard deviation, and distribution were determined.

The prototypes were then loaded under compression using a Testometric universal loading machine (M350-20CT) with a 100 kg load cell (Serial Number: 31931) (see supplementary information). One set of two black spots were drawn in the axial direction and two sets of two black spots were drawn in the transverse direction using a black marker. The markings represented the edges of a unit-cell of the system and were used to record the deformations. A compressive strain of circa 7 % was then slowly applied on the prototype with the deformation being recorded with a duly calibrated Messphysik-Video extensiometer camera. The change in lengths were monitored using the pattern recognition feature found within the video extensometer software. This yielded one measurement of the change in length in the axial direction and another two for the transverse direction from which the Poisson's ratio was then determined.

3. Results and discussion

A number of the 3D structures obtained when using diamond shaped perforations as an example of the novel design method proposed in this in this study were found to exhibit a negative Poisson's ratio in a number of perpendicular planes (see Fig. 4 and Fig. 5). The notion of using perforations (i.e., continuous pores in the third direction) in multiple planes for the design of 3D auxetic structures is not limited to the adoption of diamond shaped perforations. Other types of perforation shapes such as elliptical, rectangular, stadium and I-shaped perforations can be expected to lead to 3D auxetic structures when perforations are performed in multiple planes. An illustration of such a structures is given in Fig. 2. Referring to Fig. 2(a), elliptical perforations result in a system which projections in 3D may be described by the rotating squares mechanism. Using rectangular shaped perforations results in a 3D structure which projections in the major planes may be describe by the anti-tetrachiral mechanism (Fig. 2(b)). Using stadium shaped perforations also results in a 3D system which projections in the major planes may be described by the rotating squares mechanism (Fig. 2 (c)) while using I shaped perforations results in a 3D structure which projections in the major planes may be described by the anti-tetrachiral mechanism (Fig. 2(d)). Although numerous structures can be obtained using this novel design method, the rest of the discussion will focus on the properties obtained when diamond shaped perforations are used.

The first set of results that will be presented relate to the regular 3D perforated systems. For a constant side length of the rhombi, the pore size of this structure can be controlled by changing the angle θ, whereby the larger the value of θ the larger the pore size. This change in pore size will be accompanied by a change in the structures' volume fraction. As it may be anticipated, an increase in θ will result in a decrease of the volume fraction of the regular 3D perforated system. This is clearly shown in Fig. 3(a) were the change in volume fraction with respect to θ for systems produced from perforations having side lengths (a) of 10.0 mm separated from each other by a distance (s) of 0.5 mm are shown. It is interesting to note that the relation between the volume fraction and the angle θ is not linear. In fact for small values of θ, an increase in this angle is followed by a relatively large decrease in the material volume fraction whilst for large values of θ, an increase in this angle is followed by a relatively small change in the materials' volume fraction. This is related to the change in volume of the diamond shaped perforations, although it cannot be directly calculated by subtracting the volume of the diamond perforations from the volume of the material. The reason being that there are regions of overlap between the different perforations performed on the different planes.

Further analysis shows that the shape of the polygons resulting from the perforations vary as a function of θ. A system produced by diamond perforations having a very small angle θ may be described as cubes connected through their vertices. As the aperture angle increases, systems composed of irregular dodecahedra connected at their vertices are obtained, while when θ is 90°, the system may be described as being made of rhombic dodecahedron connected through their vertices. The vertices are highlighted through arrows in Fig. 3.(b). It is interesting to note that the resulting polygons are always connected from six vertices. Furthermore, the connectivity area between any two adjacent polygons is s^2, i.e. it is independent of angle θ. In the case that θ is approaching zero, i.e.

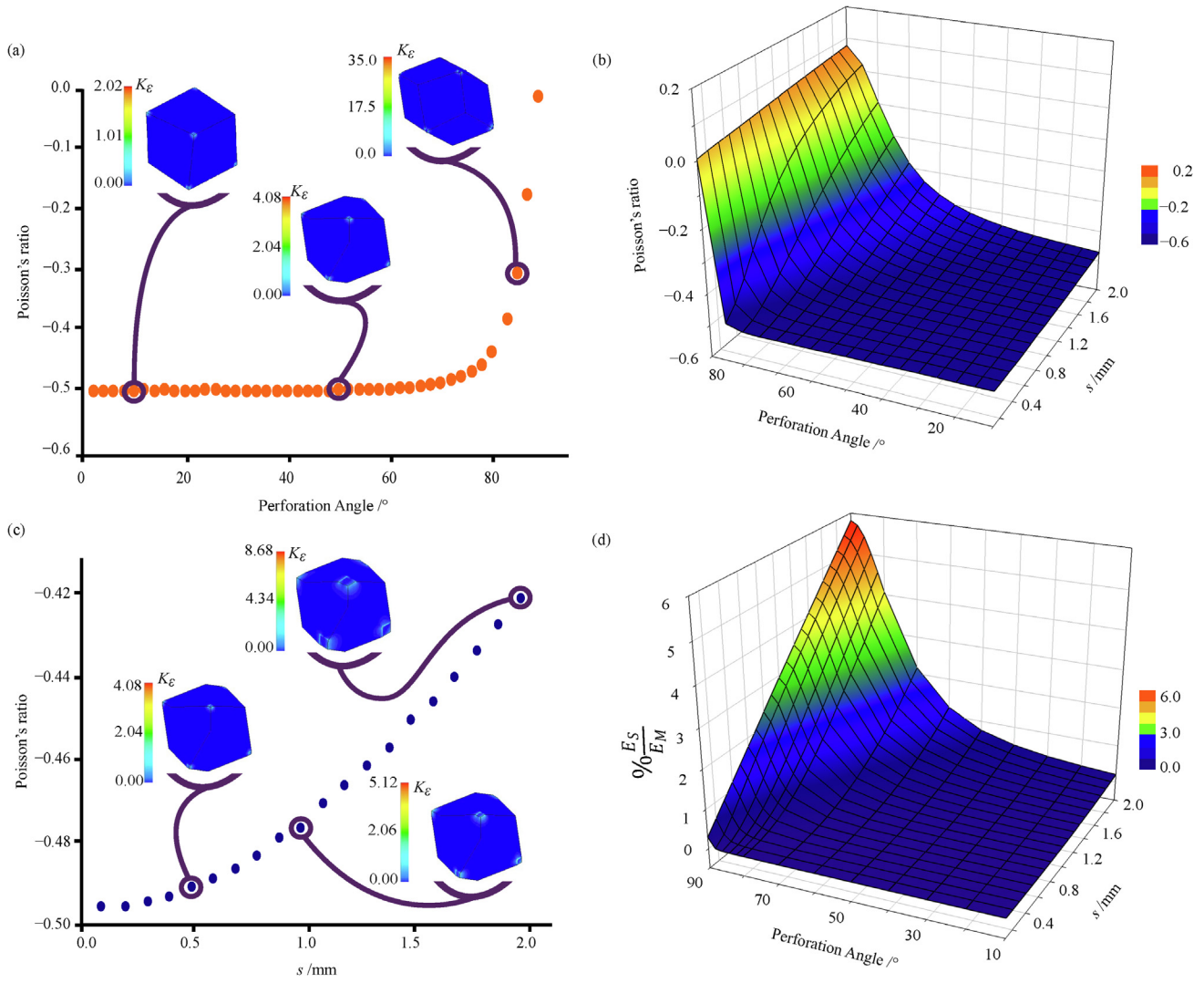

Fig. 4. Results for the regular 3D perforated system (a) The Poisson's ratio against θ (b) A 3D plot of the Poisson's ratio for the various combinations of s and θ values (c) The Poisson's ratio against parameter, s, whenθ = 50°. (d) A 3D plot depicting the percentage change in the ratio between the Young's modulus of the structure and that of the material for the various combinations of s and θ.

the polygon is approaching the shape of a cube, two vertices from each cube will not be connected. On the other hand, in the region where the shape of the polygon may be described as an irregular dodecahedron (i.e. for large θ), eight vertices will not be connected.

The variation of the Poisson's ratios and Young's moduli with θ and s for the regular 3D perforated systems are shown in Fig. 4. Given the symmetry of the structure, its mechanical properties are the same in the *xy*, *yz*, and *zx* planes. Thus, only those for the *xy* plane will be discussed in detail. With this in mind, it is evident from Fig. 4(a) that for the regular system having s = 0.5 mm, a negative Poisson's ratio of circa −0.5 is attained when the values of θ vary between 0° and 70°. Within this range of θ, the material between the perforations is primarily acting as a hinge, allowing the polygons to rotate in three dimensions when a uniaxial load is applied. This can be verified from the Cartesian axis stress distributions of the material between the perforations, which is in tension on one edge and in compression on the opposite edge (see supplementary information).

As the value of θ starts to approach 90°, the rotation of the polygons becomes more difficult. In fact, when θ is equal to 90° the polygons are unable to rotate because the geometry is such that the hinges are aligned along the line of action of the applied uniaxial force. At this point, there could be the expectation that the Poisson's ratio of the structure would be equal to that of the constituting material in view of the fact that the rotation mechanism cannot operate. However, the numerical results obtained indicate otherwise, with the Poisson's ratio of the structure approaching zero as θ approaches 90°. This indicates that a second deformation mechanism is operating. In fact, when θ is equal to 90° the perforated system can be compared to a system composed of rigid units connected through springs. A uniaxial tensile load (aligned parallel to the springs) applied on this configuration would result in the stretching of the springs, elongating them in one direction, while, at the same time, having a minimal effect, if at all, on the rest of the structure (see supplementary information). The net effect is that the configuration would exhibit a Poisson's ratio of zero. Considering that the induced deformation is localised, this mechanism will henceforth be referred to as the connection point elongation mechanism. It should be noted that in this confirmation, the connection points between the polygons will experience high internal stresses and strains. This can be verified from Fig. 4 where it can be observed that the strain concentration factor at the connection points increases dramatically as θ increases. For instance, when s = 0.5 mm the maximum strain concentration fac-

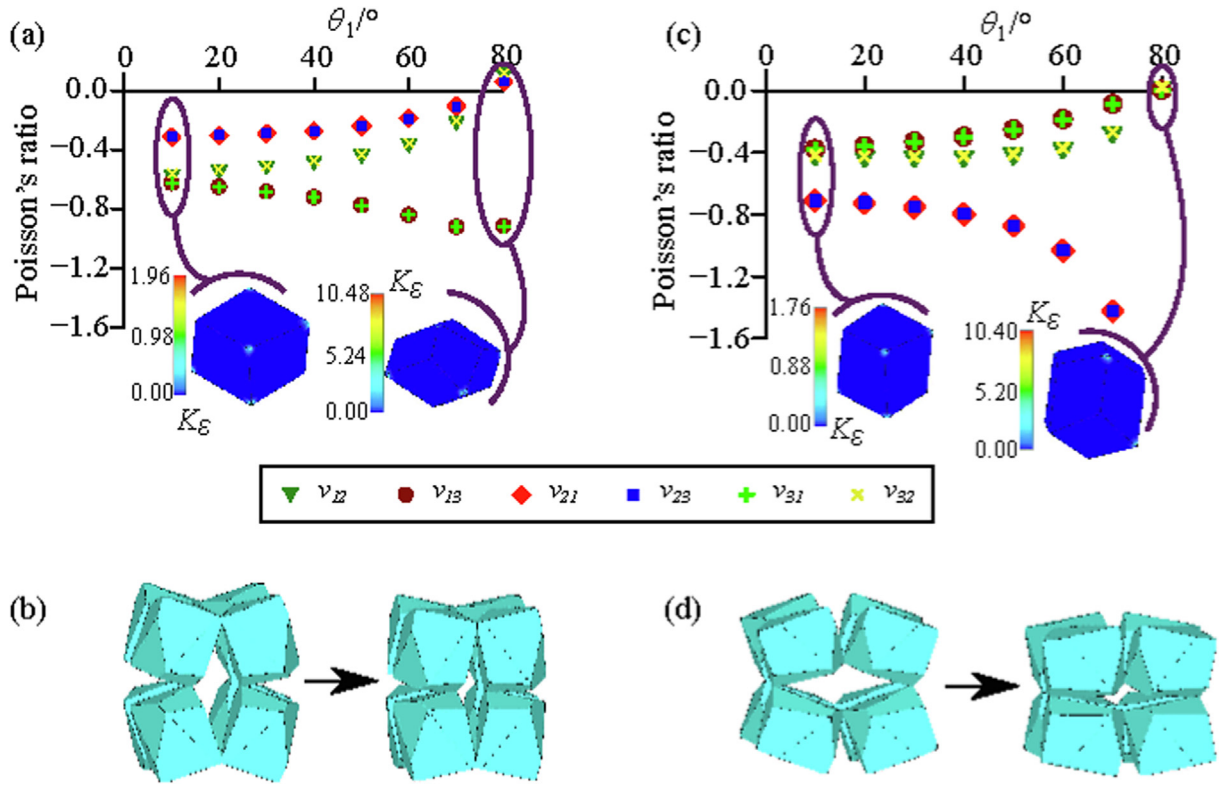

Fig. 5. (a) Poisson's ratio against θ_1 for the general 3D perforated systems having $b = c = 8.0$ mm and (b) the undeformed and deformed structures for this system when $\theta_1 = 40°$. (c) Poisson's ratio against θ_1 when $b = c = 12.0$ mm and (d) the undeformed and deformed structures for this system when $\theta_1 = 40°$. In all cases, $a = 10.0$ mm and $s = 0.5$ mm.

tor increases from 2.0 when θ is 10°to 4.1 when θ is 50° to 35.0 when θ is 85° (see Fig. 4 and supplementary information). This is also indicative that as θ increases, the probability of the structure failing at the connection points increases due to the fact that the strain (and stress) experienced by the material in these regions would be relatively large.

The stiffness of the connection between rigid units certainly plays a role in the deformation mechanism. In order to investigate this, a set of simulations were undertaken whereby the diamond shaped perforations are situated at a larger distance from each other i.e., the parameter s was increased for a number of fixed angles θ. The results indicate that up to moderately small θ (circa 50°) the Poisson's ratio is not affected to a large degree when s is increased from 0.1 to 2.0 mm. For example, when $\theta = 50°$ it changes from −0.495 to −0.419 (see Fig. 4(c)). On the other hand, for relatively large perforation angles the changes in Poisson's ratio can be significant. For example, in the case that $\theta = 86°$ the Poisson's ratio changes from −0.479 to −0.039 when s increases from 0.1 to 2.0 mm. Yet, close to the fully open system ($\theta = 90°$), the variation can be small again. For example, when $\theta = 90°$, the Poisson's ratio changes from 0.004 when $s = 0.1$ mm to 0.076 when $s = 2.0$ mm. The way that the Poisson's ratio varies with s and the perforation angle may be understood by taking into consideration the strain concentration factor plots presented in Fig. 4(c) and the von Mises stress distribution made available in the supplementary information. These plots indicate that an increase in s is accompanied by a progressive propagation of the deformation of the polyhedrons beyond the connection point. As expected, the stresses in the immediate vicinity of the connection points turn out to be different from those experienced in the rest of the polyhedron. The larger the value of s, the large the region of the polyhedron which is acting as the 'immediate vicinity' of the point of application of load onto the polyhedron. As s increases, the local deformation at the connection points extends to the bulk of the polyhedrons, something that can be considered as a 'third deformation mechanism'. The deformation of the polygons can be predicted to lead to a positive Poisson's ratio (assuming that the constituting material has a positive Poisson's ratio). In fact, it is expected to approach that of the constituent material as the size of the pores decrease in relation to the unit cell, something that progressively occurs as s increases. In consequence, the observed Poisson's ratio will be determined through the interplay of these mechanisms acting together.

The degree to which these three types of deformation mechanisms operate will also have an effect on the Young's moduli of the perforated systems proposed here. When s is small, i.e. when the perforated system is mainly deforming through the rotation and connection point deformation mechanisms, the change in the ratio $\%\frac{E_S}{E_M}$ ($=\frac{E_S}{E_M} \times 100\,\%$, where E_S and E_M are respectively the Young's moduli of the structure and the constituting material, see Fig. 4(d)), is always less than 1 % across the range of perforation angle. In fact, for $s = 0.1$ mm the $\%\frac{E_S}{E_M}$ changes from 2.97×10^{-5}% when $\theta = 10°$ to 2.96×10^{-1}% when $\theta = 90°$. On the other hand, the Young's modulus of the system changes to higher percentages when s is larger. For example, when $s = 2.0$ mm the $\%\frac{E_S}{E_M}$ changes from 2.11×10^{-1}% when $\theta = 10°$ to 5.81 % when $\theta = 90°$.

In addition to the range of configurations that can be attained by altering s and θ, the perforation of a cuboid using different sized diamonds (see Fig. 1) can result in a plethora of structures having a diverse range of mechanical properties (see supplementary information). In the cases when $a \neq b \neq c$, the projections of the structures in the xy, xz, and yz planes may be described as rectangles connected through their corners, albeit the dimensions of the pro-

jected rectangles may be different in different planes. In general, it was observed that such structures exhibited an NPR in at least one direction, the magnitude of which can be relatively large in some cases. From the sets of parameters tested in this study, the most auxetic 3D perforated system (having a = 10 mm, b = 12 mm, c = 10 mm and θ = 70°) had a Poisson's ratio of −13.14 in the zy plane, for loading in the z direction.

Comprehensive analysis of the result indicated that the deformation of these cuboidal perforated systems is similar to that of the regular 3D perforated system. When the structures are not fully open and s is relatively small they deform mainly through the relative rotation of the polygons (see Fig. 5 and supplementary information). Furthermore, the Young's moduli in the x, y, and z directions were observed to increase to a small extent when the perforation angle θ_1 and/or the ratio b/a increased. This indicates that the connection point elongation mechanism starts to operate when these parameters have large values.

Partial symmetry in the general systems can be attained when any two of the dimensions a, b, and c are equal. In this case, the initial block has the shape of a square cuboid. The resultant perforated system has a projection in one plane that may be described as squares connected through their corners, whilst in the other two planes, the projections may be described as rectangles connected through their corners. These systems showed a negative Poisson's ratio in all planes investigated (see Fig. 5).

The linear numerical results presented above were also compared to the corresponding nonlinear simulations. In the case of the regular 3D perforated system (System I), the structure showed an initial negative Poisson's ratio of −0.44 in all planes studied, as predicted by the linear simulations performed earlier. Furthermore, the nonlinear simulations indicate that the Poisson's ratio of this system is strain independent up to the maximum compression used in this study (7 % of the original length; see Fig. 6).

Analysis of the more general cuboid system (System II) gives a similar result whereby the initial Poisson's ratios ν_{ij} are in line with those determined from the linear simulations. More specifically, the values for ν_{xy}, ν_{yx}, ν_{xz}, ν_{zx}, ν_{yz} and ν_{zy} were found to be −0.260, −0.718, −0.305, −0.427, −0.678 and −0.415 respectively. Once again, the Poisson's ratios obtained for the various planes were strain independent up to the maximum strain used in this study. This is a very important result as invariance in Poisson's ratio with strain is rather uncommon amongst auxetic systems mainly due to the fact that during the deformation there is a change in geometry usually resulting in a change of the ν_{ij}. Thus, these systems can be used for applications where a constant value of the Poisson's ratio is required over a relatively large strain range. Examples of such a situation include any impact absorption setups such as car bumpers and personal protective equipment.

Further analyses of the numerical results were carried out by comparing them with those obtained through the mechanical testing of the physical prototypes. As can be observed from Fig. 6 the general trends obtained from the experimental prototypes were the same as those derived from the nonlinear analysis. In fact, the experimental prototypes showed that these systems can indeed exhibit a negative Poisson's ratio that is strain independent up to a compression of 7 %. However, for both the regular 3D perforated (System I) system and the more general system (System II), the values obtained experimentally for the Poisson's ratio differed significantly from those predicted by the nonlinear simulations. In fact, for the regular 3D perforated system, the experimentally determined Poisson's ratios ν_{xy}, ν_{yz}, and ν_{zx} were measured to be −0.229, −0.224, and −0.301 respectively. These results suggest that some anisotropy is present in the regular 3D perforated system, something which was not expected based on the symmetry and the numerical results. Furthermore, in the case of the more general system, the ν_{xy}, ν_{yx}, ν_{xz}, ν_{zx}, ν_{yz}, and ν_{zy} were measured to be of −0.068, −0.471, −0.067, −0.276, −0.531, and −0.291 respectively so that these too deferred from those obtained using nonlinear simulations.

To investigate the differences between the numerical and experimental results, the actual dimensions of the 3D printed structures were measured using microscopy as described in Section 2.4. For both System I and System II there were some discrepancies between the expected perforation dimensions and the actual dimensions. In fact, s, which should have been set to 0.8 mm, was found to vary between 0.9 and 1.5 mm in the case of the System I, and between 1.0 and 1.4 mm in the case of System II. This problem probably arose due to the poor drainage of the uncured resin from the edges of the perforations while cleaning the model with isopropanol. The extra resin, which did not drain during the cleaning phase, then cured at the intersections during the post curing stage. A change in s is not expected to cause a large change in the Poisson's ratio. However, this change in s is necessarily accompanied with a change in the dimensions of the perforations. Indeed, in the case of System I, a was found to vary between 3.7 and 4.3 mm whilst in the case of System II, a varied between 3.7 and 4.3 mm while b ranged between 4.5 and 5.1 mm. This means that in the case of System I, the perforations were not of the same dimension leading to an anisotropic behaviour of the structure. Similarly, the deviations of a and b from the intended ones can explain the discrepancies obtained between the simulated and experimental values. Such production problems can be resolved in different ways. When using additive manufacturing, the shape of the perforation can be optimised. For example, using ellipse shaped perforations instead of diamond ones allows for better resin drainage. This would require further research to study any changes in the mechanical properties because of this change in perforation shape. The proposed systems could also be produced using casting methods. This is possible as the pores in this 3D system are continuous and thus allow for the design of a mould with removable rods to produce the perforated system discussed in this study (see supplementary information for an example of such mould). Once casting is complete one would simply remove the rods and obtain the system which was investigated in this study. The systems investigated in this study could also be produced by a subtractive method. Subtractive methods are generally easier to implement than additive manufacturing, however, they may be less cost-effective due to material wastage. When using subtractive methods, the cost effectiveness would highly depend on the size of the perforations. For example, in the case of the regular 3D perforated system, using small values for angle θ will result in 'slit' like perorations. Production of such a system using subtractive methods will probably be cost effective as minimal material loss will occur. On the other hand, if large values for angle θ are used, subtractive methods may not be cost effective due to the large amount of lost material. This may be clearly inferred form Fig. 3 where the volume fraction of the regular system for various values of θ is given.

Before concluding it is also important to point out that the 3D structures that result when using this novel design method with diamond shaped perforations are also novel. First and foremost, such 3D structures can be fabricated using a number of fabrication methodologies. This is due to the fact that the perforations extend across the whole length of the cuboid in the x, y, and z directions (continuous voids of constant cross-sectional area). Thus, such systems can be produced through casting by creating a mould chamber having interpenetrating and detachable diamond-shaped rods. The assembled mould itself would constitute the negative image of the perforated cuboid just presented with the diamond shaped rods creating the necessary voids (see supplementary information). Furthermore, because of the presence of the continuous voids of constant cross-sectional area, these systems can also be produced

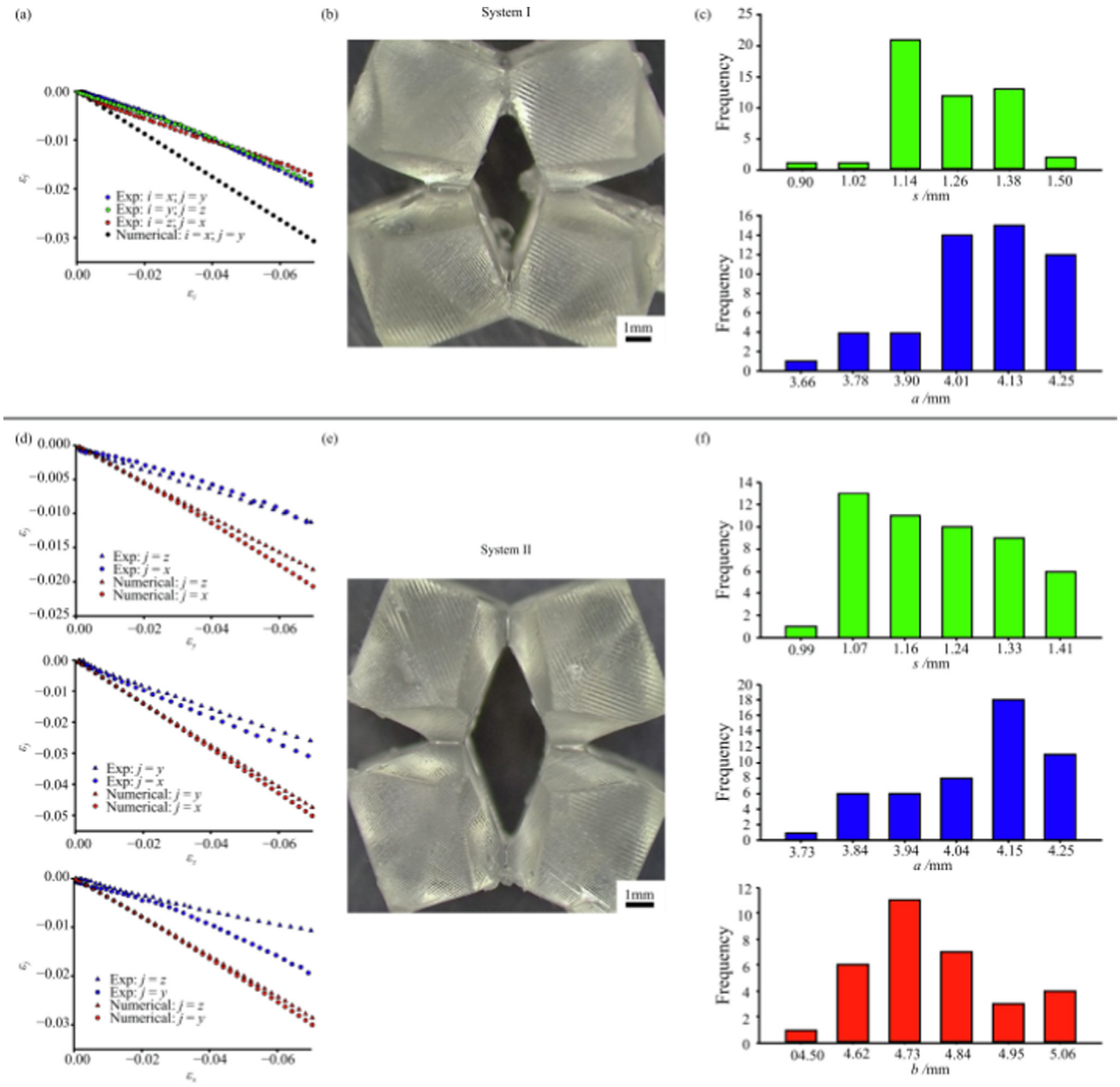

Fig. 6. Comparison of the Poisson's ratio between the experimental and non-linear numerical results for (a) System I and (d) System II. Part of the experimental prototype of (b) System I and. (e) System II. Frequency distribution graphs for different parameters of (c) System I and (f) System II.

through subtractive manufacturing. Such 3D systems would also show advantages when using additive manufacturing as they would have a clear drainage channel thus eliminating issues such as cupping.

Furthermore, the results obtained suggest that these 3D systems have a strain independent Poisson's ratio (up to the maximum strain used in this study). This is a desirable feature which is not obtained in numerous auxetic structures. For example, the 2D perforated systems that mimic the re-entrant honeycomb systems [72] do not exhibit a strain independent Poisson's ratio. Moreover, the systems designed using equally sized diamond shaped perforations (the regular 3D perforated systems) where shown to have a nearly constant Poisson's ratio for a large degree of θ values (up to 60°). This is not the case for other 3D rotating polygons. For example, the rotating cubes proposed by Kim et al. [36] were shown to have a Poisson's ratio that varies between -0.51 and -0.98 as the angles between the cubes change between 2° and 60°. It was also found that in the case of the 3D systems produced with diamond shaped perforations a Poisson's ratio of 0 can also be obtained when the distance between the perforations (s) is small, and θ has a value of 90°.

The perforated 3D systems proposed in this study may be used in a plethora of applications. For example, they can find use in protection equipment ranging from helmets to protective sports equipment. As discussed above, materials with a negative Poisson's ratio have superior indentation resistance since the material tends to move towards the zone of impact rather than away from it as is the case for positive Poisson's ratio materials. However, in the case of '2D' auxetic systems such as the rotating squares [1], one would expect that the material would move towards the direction of impact from only one orthogonal direction whilst in 3D auxetic systems, such as the regular 3D perforated system proposed here,

one would expect that the material moves towards the zone of impact from all orthogonal directions, hence making the material more resistant to impact. 3D materials like the ones proposed in this study would also be useful for the production of 3D actuators where an extension in the *x*-direction would result in the perpendicular motion in the *y*- and *z*-directions. Furthermore, through the design of the perforation used, one may design a system which amplifies the strain in one of the orthogonal directions. Such applications are possible as the Poisson's ratio was found to be nearly linear with applied strain (up to the maximum strain used in this study, 7 %). Furthermore, such perforated systems may find use in the production of prosthetics. For instance, recent studies have shown that tendons have a highly anisotropic Poisson's ratio, with a large negative Poisson's ratio in one plane [83]. Thus, the mechanical properties of the proposed perforated systems may be fine-tuned to those of the tendon, with the aim of producing prosthetics that mimic the behaviour of real tendons.

4. Conclusion

In this study, it was shown that a novel design method may be employed to obtain auxetic 3D structures. This method utilises the application of continuous voids of constant cross-sectional area in multiple planes. The significant innovation of this work is that it shows that perforations i.e. continuous pores within a material may be used to design 3D auxetic structures. Since the pores are continuous and have the same cross-sectional area throughout the pore, several manufacturing techniques such as additive manufacturing, subtractive manufacturing and casting techniques can be employed to produce 3D auxetic structures. Due to their pore geometry, such systems are by far easier to produce when compared to current 3D auxetic systems with complex geometries. In order to exemplify the proposed design method, several 3D structures were constructed using a series of diamond shaped perforations applied at strategic locations on multiple planes. The 3D structures obtained are also novel due to a number of characteristics which they show. The simplest structure considered here has equal sized perforation in the *xy*, *yz*, and *zx* planes. Computational simulations have shown that this configuration has a negative Poisson's ratio of circa −0.5 in the *xy*, *yz*, and *zx* planes as long as the spacing between the perforations is relatively small. Furthermore, nonlinear simulations indicate that the Poisson's ratio obtained for these systems is strain independent up to the maximum strain used in this study (7 %). Also of interest is the fact that, when the distance between the perforations is small and the perforation angle is 90°, a system with a Poisson's ratio of zero may be obtained. A more general 3D system having diamond shaped perforations was also studied, whereby different size perforation were used. The results obtained showed that an array of structures exhibiting a range of anisotropic Poisson's ratios and Young's moduli can be obtained.

Furthermore, it was shown that the methodology presented in this study is not restricted to the use of diamond shaped perforations but other shapes, such as elliptical, stadium, rectanglar and I shaped perforations can be used to obtain structures that can lead to auxetic behaviour. Thus, it can be envisioned that this work can promote the development of manufacturing methods for the low-cost production of 3D auxetic systems making their industrial use in numerous areas possible.

Data availability

Data will be made available on request.

Declaration of Competing Interest

The authors declare that they have no known competing financial interests or personal relationships that could have appeared to influence the work reported in this paper.

Acknowledgments

The research work disclosed in this publication was funded by the Tertiary Education Scholarship Scheme (Malta). It also made use of the computational facilities procured through the European Regional Development Fund, Project ERDF-080 'A supercomputing laboratory for the University of Malta' and the University of Malta Academic Work Resources Fund. Images used courtesy of ANSYS, Inc.

Appendix A. Supplementary material

Supplementary data to this article can be found online at https://doi.org/10.1016/j.matdes.2023.111596.

References:

[1] J.N. Grima, K.E. Evans, Auxetic behavior from rotating squares, J. Mater. Sci. Lett. 19 (2000) 1563–1565, https://doi.org/10.1023/A:1006781224002.
[2] Z.G. Nicolaou, A.E. Motter, Mechanical metamaterials with negative compressibility transitions, Nature Materials 2012 11:7. 11 (2012) 608–613. https://doi.org/10.1038/nmat3331.
[3] T.A.M. Hewage, K.L. Alderson, A. Alderson, F. Scarpa, T.A. M Hewage, K.L. Alderson, A. Alderson, F.T. Scarpa A M Hewage, A. Alderson, K.L. Alderson, P. Lane, F. Scarpa, Double-Negative Mechanical Metamaterials Displaying Simultaneous Negative Stiffness and Negative Poisson's Ratio Properties, Advanced Materials. 28 (2016) 10323–10332. https://doi.org/10.1002/adma.201603959.
[4] W. Yang, Z.-M. Li, W. Shi, B.-H. Xie, M.-B. Yang, Review On auxetic materials, n. d.
[5] K.E. Evans, Auxetic polymers: a new range of materials, Endeavour 15 (1991) 170–174, https://doi.org/10.1016/0160-9327(91)90123-S.
[6] J.N. Grima, P.S. Farrugia, C. Caruana, R. Gatt, D. Attard, Auxetic behaviour from stretching connected squares, J. Mater. Sci. 43 (2008) 5962–5971, https://doi.org/10.1007/s10853-008-2765-0.
[7] J.B. Choi, R.S. Lakes, Non-linear properties of metallic cellular materials with a negative Poisson's ratio, J. Mater. Sci. 27 (1992) 5375–5381, https://doi.org/10.1007/BF02403846.
[8] V.L. Coenen, K.L. Alderson, Mechanisms of failure in the static indentation resistance of auxetic carbon fibre laminates, Physica Status Solidi (B) Basic Research 248 (2011) 66–72, https://doi.org/10.1002/pssb.201083977.
[9] I.I. Argatov, R. Guinovart-Díaz, F.J. Sabina, On local indentation and impact compliance of isotropic auxetic materials from the continuum mechanics viewpoint, Int. J. Eng. Sci. 54 (2012) 42–57, https://doi.org/10.1016/j.ijengsci.2012.01.010.
[10] K.K. Dudek, W. Wolak, R. Gatt, J.N. Grima, Impact resistance of composite magnetic metamaterials, Sci. Rep. 9 (2019) 65–69, https://doi.org/10.1038/s41598-019-40610-w.
[11] J.B. Choi, Fracture toughness of re-entrant foam materials with a negative Poisson's ratio: experiment and analysis, Int. J. Fract. 80 (1996) 73–83, https://doi.org/10.1007/BF00036481.
[12] G. Imbalzano, P. Tran, T.D. Ngo, P.V.S. Lee, A numerical study of auxetic composite panels under blast loadings, Compos. Struct. 135 (2016) 339–352, https://doi.org/10.1016/j.compstruct.2015.09.038.
[13] L. Jiang, H. Hu, Low-velocity impact response of multilayer orthogonal structural composite with auxetic effect, Compos. Struct. 169 (2017) 62–68, https://doi.org/10.1016/j.compstruct.2016.10.018.
[14] S. Hou, T. Liu, Z. Zhang, X. Han, Q. Li, How does negative Poisson's ratio of foam filler affect crashworthiness?, Mater Des. 82 (2015) 247–259, https://doi.org/10.1016/j.matdes.2015.05.050.
[15] A. Alderson, J. Rasburn, S. Ameer-Beg, P.G. Mullarkey, W. Perrie, K.E. Evans, An auxetic filter: A tuneable filter displaying enhanced size selectivity or defouling properties, Ind. Eng. Chem. Res. 39 (2000) 654–665, https://doi.org/10.1021/ie990572w.
[16] T. Allen, T. Hewage, C. Newton-Mann, W. Wang, O. Duncan, A. Alderson, Fabrication of auxetic foam sheets for sports applications, Physica Status Solidi (B) Basic Research 254 (2017) 1700596, https://doi.org/10.1002/pssb.201700596.
[17] Z. Wang, A. Zulifqar, H. Hu, Auxetic composites in aerospace engineering, in: Advanced Composite Materials for Aerospace Engineering, Elsevier, 2016, pp. 213–240, https://doi.org/10.1016/b978-0-08-100037-3.00007-9.
[18] M. Sanami, N. Ravirala, K. Alderson, A. Alderson, Auxetic materials for sports applications, Procedia Engineering, Elsevier Ltd, 2014, pp. 453–458.

[19] F. Scarpa, Auxetic materials for bioprostheses, IEEE Signal Process Mag. 25 (2008), https://doi.org/10.1109/MSP.2008.926663.
[20] J. Zeng, H. Hu, L. Zhou, A study on negative Poisson's ratio effect of 3D auxetic orthogonal textile composites under compression, Smart Mater. Struct. 26 (2017), https://doi.org/10.1088/1361-665X/aa6fe6.
[21] M. Liaqat, H.A. Samad, S.T.A. Hamdani, Y. Nawab, The development of novel auxetic woven structure for impact applications, J. Text. Inst. 108 (2017) 1264–1270, https://doi.org/10.1080/00405000.2016.1239330.
[22] K.K. Dudek, R. Gatt, M.R. Dudek, J.N. Grima, Negative and positive stiffness in auxetic magneto-mechanical metamaterials, Proceedings of the Royal Society A: Mathematical, Physical and Engineering Sciences. 474 (2018). https://doi.org/10.1098/rspa.2018.0003.
[23] K.K. Dudek, R. Gatt, J.N. Grima, 3D composite metamaterial with magnetic inclusions exhibiting negative stiffness and auxetic behaviour, Mater. Des. 187 (2020), https://doi.org/10.1016/j.matdes.2019.108403 108403.
[24] Y. Ma, F. Scarpa, D. Zhang, B. Zhu, L. Chen, J. Hong, A nonlinear auxetic structural vibration damper with metal rubber particles, Smart Mater. Struct. 22 (2013), https://doi.org/10.1088/0964-1726/22/8/084012.
[25] S.L. Zhang, Y.C. Lai, X. He, R. Liu, Y. Zi, Z.L. Wang, Auxetic foam-based contact-mode triboelectric nanogenerator with highly sensitive self-powered strain sensing capabilities to monitor human body movement, Adv. Funct. Mater. 27 (2017) 1–7, https://doi.org/10.1002/adfm.201606695.
[26] Q. Li, Y. Kuang, M. Zhu, Auxetic piezoelectric energy harvesters for increased electric power output, AIP Adv. 7 (2017), https://doi.org/10.1063/1.4974310.
[27] Y.C. Wang, R. Lakes, Analytical parametric analysis of the contact problem of human buttocks and negative Poisson's ratio foam cushions, Int. J. Solids Struct. 39 (2002) 4825–4838, https://doi.org/10.1016/S0020-7683(02)00379-7.
[28] F. Warmuth, F. Osmanlic, L. Adler, M.A. Lodes, C. Körner, Fabrication and characterisation of a fully auxetic 3D lattice structure via selective electron beam melting, Smart Mater. Struct. 26 (2017), https://doi.org/10.1088/1361-665X/26/2/025013.
[29] K. Bertoldi, P.M. Reis, S. Willshaw, T. Mullin, Negative poisson's ratio behavior induced by an elastic instability, Adv. Mater. 22 (2010) 361–366, https://doi.org/10.1002/adma.200901956.
[30] K.K. Dudek, W. Wolak, M.R. Dudek, R. Caruana-Gauci, R. Gatt, K.W. Wojciechowski, J.N. Grima, Programmable magnetic domain evolution in magnetic auxetic systems, Physica Status Solidi - Rapid Research Letters. 11 (2017) 1–6, https://doi.org/10.1002/pssr.201700122.
[31] J.N. Grima, R. Caruana-Gauci, M.R. Dudek, K.W. Wojciechowski, R. Gatt, Smart metamaterials with tunable auxetic and other properties, Smart Mater. Struct. 22 (2013) 084016.
[32] M.R. Dudek, K.W. Wojciechowski, Magnetic films of negative Poisson's ratio in rotating magnetic fields, J. Non Cryst. Solids 354 (2008) 4304–4308, https://doi.org/10.1016/j.jnoncrysol.2008.06.086.
[33] K.L. Alderson, V.R. Simkins, V.L. Coenen, P.J. Davies, A. Alderson, K.E. Evans, How to make auxetic fibre reinforced composites, Physica Status Solidi (B) Basic Research. 242 (2005) 509–518. https://doi.org/10.1002/pssb.200460371.
[34] A. Bezazi, F. Scarpa, Tensile fatigue of conventional and negative Poisson's ratio open cell PU foams, Int. J. Fatigue 31 (2009) 488–494, https://doi.org/10.1016/j.ijfatigue.2008.05.005.
[35] D. Attard, J.N. Grima, A three-dimensional rotating rigid units network exhibiting negative Poisson's ratios, Physica Status Solidi (B) Basic Research. 249 (2012) 1330–1338. https://doi.org/10.1002/pssb.201084223.
[36] J. Kim, D. Shin, D.-S. Yoo, K. Kim, Regularly configured structures with polygonal prisms for three-dimensional auxetic behaviour, Proceedings of the Royal Society A: Mathematical, Physical and Engineering Sciences. 473 (2017) 20160926. https://doi.org/10.1098/rspa.2016.0926.
[37] T.-C. Lim, A 3D auxetic material based on intersecting double arrowheads, Physica Status Solidi (b). 253 (2016) 1252–1260, https://doi.org/10.1002/PSSB.201600015.
[38] L. Yang, O. Harrysson, H. West, D. Cormier, Compressive properties of Ti–6Al–4V auxetic mesh structures made by electron beam melting, Acta Mater. 60 (2012) 3370–3379, https://doi.org/10.1016/J.ACTAMAT.2012.03.015.
[39] K. Wang, Y.H. Chang, Y.W. Chen, C. Zhang, B. Wang, Designable dual-material auxetic metamaterials using three-dimensional printing, Mater. Des. 67 (2015) 159–164, https://doi.org/10.1016/J.MATDES.2014.11.033.
[40] P.S. Farrugia, R. Gatt, J.N. Grima, A Novel Three-Dimensional Anti-Tetrachiral Honeycomb, Physica Status Solidi (B) Basic Research. 256 (2019) 1–10. https://doi.org/10.1002/pssb.201800473.
[41] C.S. Ha, M.E. Plesha, R.S. Lakes, Chiral three-dimensional lattices with tunable Poisson's ratio, Smart Mater. Struct. 25 (2016), https://doi.org/10.1088/0964-1726/25/5/054005 054005.
[42] J.W. Narojczyk, K.W. Wojciechowski, K.V. Tretiakov, J. Smardzewski, F. Scarpa, P.M. Piglowski, M. Kowalik, A.R. Imre, M. Bilski, Auxetic properties of a f.c.c. crystal of hard spheres with an array of [001]-nanochannels filled by hard spheres of another diameter, Physica Status Solidi (b) 256 (2019) 1800611, https://doi.org/10.1002/pssb.201800611.
[43] K.V. Tretiakov, P.M. Piglowski, K. Hyzorek, K.W. Wojciechowski, Enhanced auxeticity in Yukawa systems due to introduction of nanochannels in [001]-direction, Smart Mater. Struct. 25 (2016), https://doi.org/10.1088/0964-1726/25/5/054007 054007.
[44] D.T. Ho, C.T. Nguyen, S.-Y. Kwon, S.Y. Kim, Auxeticity in metals and periodic metallic porous structures induced by elastic instabilities, Physica Status Solidi (b). 256 (2019) 1800122, https://doi.org/10.1002/pssb.201800122.
[45] D.R. Reid, N. Pashine, A.S. Bowen, S.R. Nagel, J.J. de Pablo, Ideal isotropic auxetic networks from random networks, Soft Matter 15 (2019) 8084–8091, https://doi.org/10.1039/C9SM01241A.
[46] S. Babaee, J. Shim, J.C. Weaver, E.R. Chen, N. Patel, K. Bertoldi, 3D soft metamaterials with negative Poisson's ratio, Adv. Mater. 25 (2013) 5044–5049, https://doi.org/10.1002/ADMA.201301986.
[47] J. Shim, C. Perdigou, E.R. Chen, K. Bertoldi, P.M. Reis, Buckling-induced encapsulation of structured elastic shells under pressure, Proc. Natl. Acad. Sci. 109 (2012) 5978–5983, https://doi.org/10.1073/PNAS.1115674109.
[48] T.D. Ngo, A. Kashani, G. Imbalzano, K.T.Q. Nguyen, D. Hui, Additive manufacturing (3D printing): A review of materials, methods, applications and challenges, Compos. B Eng. 143 (2018) 172–196, https://doi.org/10.1016/j.compositesb.2018.02.012.
[49] J.N. Grima, R. Gatt, Perforated sheets exhibiting negative Poisson's ratios, Adv. Eng. Mater. 12 (2010) 460–464, https://doi.org/10.1002/adem.201000005.
[50] J.N. Grima, R. Gatt, B. Ellul, E. Chetcuti, Auxetic behaviour in non-crystalline materials having star or triangular shaped perforations, J. Non Cryst. Solids 356 (2010) 1980–1987, https://doi.org/10.1016/j.jnoncrysol.2010.05.074.
[51] D. Attard, R. Caruana-Gauci, R. Gatt, J.N. Grima, Negative linear compressibility from rotating rigid units, Physica Status Solidi (B) Basic Research. 253 (2016) 1410–1418. https://doi.org/10.1002/pssb.201600092.
[52] F. Scarpa, W.A. Bullough, P. Lumley, Trends in acoustic properties of iron particle seeded auxetic polyurethane foam, Proceedings of the Institution of Mechanical Engineers, Part C: Journal of Mechanical Engineering Science. 218 (2004) 241–244. https://doi.org/10.1243/095440604322887099.
[53] A. Slann, W. White, F. Scarpa, K. Boba, I. Farrow, Cellular plates with auxetic rectangular perforations, Physica Status Solidi (B) Basic Research. 252 (2015) 1533–1539. https://doi.org/10.1002/pssb.201451740.
[54] J.N. Grima, L. Mizzi, K.M. Azzopardi, R. Gatt, Auxetic Perforated Mechanical Metamaterials with Randomly Oriented Cuts, Adv. Mater. 28 (2016) 385–389, https://doi.org/10.1002/adma.201503653.
[55] H. Wang, S.H. Xiao, C. Zhang, Novel planar auxetic metamaterial perforated with orthogonally aligned oval-shaped holes and machine learning solutions, Adv. Eng. Mater. (2021) 2100102, https://doi.org/10.1002/adem.202100102.
[56] R.J. Nedoushan, W.R. Yu, A new auxetic structure with enhanced stiffness via stiffened elliptical perforations, Functional Compos. Struct. 2 (2020), https://doi.org/10.1088/2631-6331/abd373 045006.
[57] J. Yao, R. Sun, F. Scarpa, C. Remillat, Y. Gao, Y. Su, Two-dimensional graded metamaterials with auxetic rectangular perforations, Compos. Struct. 261 (2021), https://doi.org/10.1016/j.compstruct.2020.113313 113313.
[58] S. Linforth, T. Ngo, P. Tran, D. Ruan, R. Odish, Investigation of the auxetic oval structure for energy absorption through quasi-static and dynamic experiments, Int. J. Impact Eng 147 (2021), https://doi.org/10.1016/j.ijimpeng.2020.103741 103741.
[59] L. Mizzi, D. Attard, K.E. Evans, R. Gatt, J.N. Grima, Auxetic mechanical metamaterials with diamond and elliptically shaped perforations, Acta Mech. 232 (2021) 779–791, https://doi.org/10.1007/s00707-020-02881-7.
[60] J.N. Grima, K.E. Evans, Auxetic behavior from rotating triangles, (2006). https://doi.org/10.1007/s10853-006-6339-8.
[61] E. Chetcuti, B. Ellul, E. Manicaro, J.P. Brincat, D. Attard, R. Gatt, J.N. Grima, Modeling auxetic foams through semi-rigid rotating triangles, Physica Status Solidi (B) Basic Research 251 (2014) 297–306, https://doi.org/10.1002/pssb.201384252.
[62] J.N. Grima, R. Gatt, A. Alderson, K.E. Evans, On the auxetic properties of "rotating rectangles" with different connectivity, J. Phys. Soc. Jpn. 74 (2005) 2866–2867, https://doi.org/10.1143/JPSJ.74.2866.
[63] D. Attard, E. Manicaro, J.N. Grima, On rotating rigid parallelograms and their potential for exhibiting auxetic behaviour, Physica Status Solidi (B) Basic, Research 246 (2009) 2033–2044, https://doi.org/10.1002/pssb.200982034.
[64] A. Alderson, K.L. Alderson, D. Attard, K.E. Evans, R. Gatt, J.N. Grima, W. Miller, N. Ravirala, C.W. Smith, K. Zied, Elastic constants of 3-, 4- and 6-connected chiral and anti-chiral honeycombs subject to uniaxial in-plane loading, Compos. Sci. Technol. 70 (2010) 1042–1048, https://doi.org/10.1016/j.compscitech.2009.07.009.
[65] D. Prall, R.S. Lakes, Properties of a chiral honeycomb with a Poisson's ratio-1, J. Mech. Sci. (1996).
[66] L. Mizzi, D. Attard, R. Gatt, P.S. Farrugia, J.N. Grima, An analytical and finite element study on the mechanical properties of irregular hexachiral honeycombs, Smart Mater. Struct. 27 (2018), https://doi.org/10.1088/1361-665X/aad3f6 105016.
[67] K.E. Evans, A. Alderson, F.R. Christian, Auxetic two-dimensional polymer networks. An example of tailoring geometry for specific mechanical properties, J. Chem. Soc. Faraday Trans. 91 (1995) 2671–2680, https://doi.org/10.1039/FT9959102671.
[68] I.G. Masters, K.E. Evans, Models for the elastic deformation of honeycombs, Compos. Struct. 35 (1996) 403–422, https://doi.org/10.1016/S0263-8223(96)00054-2.
[69] K.K. Dudek, R. Gatt, L. Mizzi, M.R. Dudek, D. Attard, K.E. Evans, J.N. Grima, On the dynamics and control of mechanical properties of hierarchical rotating rigid unit auxetics, Sci. Rep. 7 (2017) 1–9, https://doi.org/10.1038/srep46529.
[70] G. Wu, Y. Cho, I.S. Choi, D. Ge, J. Li, H.N. Han, T. Lubensky, S. Yang, Directing the deformation paths of soft metamaterials with prescribed asymmetric units, Adv. Mater. 27 (2015) 2747–2752, https://doi.org/10.1002/adma.201500716.
[71] M. Taylor, L. Francesconi, M. Gerendás, A. Shanian, C. Carson, K. Bertoldi, Low porosity metallic periodic structures with negative poisson's ratio, Adv. Mater. 26 (2014) 2365–2370, https://doi.org/10.1002/adma.201304464.

[72] L. Mizzi, K.M. Azzopardi, D. Attard, J.N. Grima, R. Gatt, Auxetic metamaterials exhibiting giant negative Poisson's ratios, Physica Status Solidi - Rapid Research Letters. 9 (2015) 425–430, https://doi.org/10.1002/pssr.201510178.
[73] J. Shim, S. Shan, A. Košmrlj, S.H. Kang, E.R. Chen, J.C. Weaver, K. Bertoldi, Harnessing instabilities for design of soft reconfigurable auxetic/chiral materials, Soft Matter 9 (2013) 8198–8202, https://doi.org/10.1039/c3sm51148k.
[74] L. Mizzi, E.M. Mahdi, K. Titov, R. Gatt, D. Attard, K.E. Evans, J.N. Grima, J.C. Tan, Mechanical metamaterials with star-shaped pores exhibiting negative and zero Poisson's ratio, Mater. Des. 146 (2018) 28–37, https://doi.org/10.1016/j.matdes.2018.02.051.
[75] K.W. Wojciechowski, Constant thermodynamic tension Monte Carlo studies of elastic properties of a two-dimensional system of hard cyclic hexamers, Mol. Phys. 61 (1987) 1247–1258, https://doi.org/10.1080/00268978700101761.
[76] K.W. Wojciechowski, Two-dimensional isotropic system with a negative Poisson ratio, Phys. Lett. A 137 (1989) 60–64, https://doi.org/10.1016/0375-9601(89)90971-7.
[77] D. Attard, P.S. Farrugia, R. Gatt, J.N. Grima, Starchirals – a novel class of auxetic hierarchal structures, Int. J. Mech. Sci. 179 (2020), https://doi.org/10.1016/j.ijmecsci.2020.105631 105631.
[78] S. Shan, S.H. Kang, Z. Zhao, L. Fang, K. Bertoldi, Design of planar isotropic negative Poisson's ratio structures, Extreme Mech. Lett. 4 (2015) 96–102, https://doi.org/10.1016/j.eml.2015.05.002.
[79] Y. Cho, J.H. Shin, A. Costa, T.A. Kim, V. Kunin, J. Li, S.Y. Lee, S. Yang, H.N. Han, I.S. Choi, D.J. Srolovitz, Engineering the shape and structure of materials by fractal cut, Proceedings of the National Academy of Sciences of the United States of America. 111 (2014) 17390–17395. https://doi.org/10.1073/pnas.1417276111.
[80] V. Kunin, S. Yang, Y. Cho, P. Deymier, D.J. Srolovitz, Static and dynamic elastic properties of fractal-cut materials, Extreme Mech. Lett. 6 (2016) 103–114, https://doi.org/10.1016/j.eml.2015.12.003.
[81] P.-S. Farrugia, R. Gatt, J.N. Grima, The push drill mechanism as a novel method to create 3D mechanical metamaterial structures, Physica Status Solidi (RRL) – Rapid Research Letters. 14 (2020) 2000125, https://doi.org/10.1002/pssr.202000125.
[82] ANSYS Inc., 2010. ANSYS Mechanical APDL Element Reference, Release 13. Pennsylvania, USA., (n.d.).
[83] R. Gatt, M. Vella Wood, A. Gatt, F. Zarb, C. Formosa, K.M. Azzopardi, A. Casha, T. P. Agius, P. Schembri-Wismayer, L. Attard, N. Chockalingam, J.N. Grima, Negative Poisson's ratios in tendons: An unexpected mechanical response, Acta Biomaterialia 24 (2015) 201–208. https://10.1016/j.actbio.2015.06.018.